Preprint

For the published version of this manuscript, please see

https://doi.org/10.1016/j.culher.2020.01.016

Journal of Cultural Heritage

Volume 44, July–August 2020, Pages 317-324

On the acid-responsive release of benzotriazole from engineered mesoporous silica nanoparticles for corrosion protection of metal surfaces

R. Castaldo [a,1], M. Salzano de Luna [b,c,1], C. Siviello [a], G. Gentile [a,*], M. Lavorgna [c,*], E. Amendola [c], M. Cocca [a]

a Institute for Polymers, Composites and Biomaterials, National Research Council of Italy, Via Campi Flegrei 34, 80078 Pozzuoli (Naples), Italy

b Department of Chemical, Materials and Production Engineering (INSTM Consortium – UdR Naples), University of Naples Federico II, Piazzale Tecchio 80, 80125 Naples, Italy

c Institute for Polymers, Composites and Biomaterials, National Research Council of Italy, Piazzale E. Fermi 1, 80055 Portici (Naples), Italy

1 These two authors contributed equally

* Corresponding Authors: G. Gentile (gennaro.gentile@cnr.it) and M. Lavorgna (marino.lavorgna@cnr.it)

Highlights

- UV-induced degradation lowers the corrosion inhibitor ability of benzotriazole
- Mesoporous silica nanocarriers protect benzotriazole from photodegradation
- High anticorrosion efficacy of nanocomposite coatings even after UV exposure

Abstract

Corrosion inhibitors are largely exploited for the development of highly performing polymeric active coatings. One of the major drawbacks, however, relies in their UV sensitivity, which may compromise their ability to effectively prevent corrosion processes. This issue is particularly relevant in the field of cultural heritage preservation, in which polymeric active coating which are able to ensure a reliable and long-lasting protection against corrosion are highly needed. Besides proving that UV-induced photodegradation impressively lowers the corrosion inhibition ability of benzotriazole (BTA), in the present work we show that this phenomenon can be largely prevented by exploiting inorganic nanocarriers. More specifically, BTA molecules loaded into functionalized mesoporous silica nanoparticles are preserved from photodegradation and released in the host coating only in the presence of acid-related external stimuli. Accelerated corrosion tests carried out on polymer nanocomposite coatings containing functionalized mesoporous silica nanoparticles loaded with BTA demonstrated that the developed system possesses an excellent anticorrosion ability.

Keywords

Benzotriazole; photodegradation; corrosion protection; coating; copper-based alloys; smart nanocarriers.

Research aim

The present work shows that that 1H-benzotriazole molecules significantly lose their corrosion inhibitor ability when subjected to UV irradiation, severely limiting their use in organic coatings intended for long-lasting protection of metal works of art and, more in general, metal surfaces. The goal of our research is to prove that this drawback can be overcome by exploiting mesoporous silica nanoparticles as smart nanocarriers able to embed the inhibitor molecules, preserving them from photodegradation, and to promote the stimuli-responsive release of the inhibitor in presence of a corrosive acid agent. Accelerated corrosion tests demonstrate that protective coatings based on BTA-loaded nanocarriers, even after prolonged exposure to UV irradiation, are extremely effective against corrosion also in highly aggressive environments.

1. Introduction

Corrosion is a serious issue for metallic materials, as it dramatically affects the stability of their properties over time. Nowadays, organic coatings represent one of the most widespread approaches for corrosion protection of metal surfaces [1]. In this field, active systems based on the use of nanocarriers loaded with corrosion inhibitor compounds emerged as an effective approach for the realization of highly performing polymeric active coatings [2] Different kinds of nanoparticles, such as halloysite nanotubes, layered double hydroxide nanoparticles, polymeric micro/nanocapsules, and mesoporous silica, have been investigated as potential carriers of anticorrosion agents to be dispersed in active coatings for the protection of metal substrates. One of the main advantages of this approach relies in the triggered and tailored release of anticorrosion molecules to contrast the chemical degradation reactions of metal substrates, which also allows to overcome possible solubility limits of corrosion inhibitors in the coating formulations. Additionally, the use of nanocarriers is useful to protect the anticorrosion additives against the exposure to environmental conditions [3-6]. However, the extension of the approaches of "classic" corrosion science to the field of cultural heritage preservation is not straightforward due to the high aesthetic and ethical demands. Nonetheless, the use of active coatings also finds large use in the field of conservation of metal works of art [7-10].
Despite their extensive exploitation, Serdechnova et al. recently raised awareness about the UV-induced photodegradation of corrosion inhibitor molecules and the resulting possible implications on the long-lasting protective ability of the resulting active coatings [11]. Actually, some of the authors of the present work showed that the anticorrosion efficacy of organic coatings containing 2-mercaptobenzothiazole (MBT) is dramatically compromised when subjected to either UV or artificial light irradiation [6]. At the same time, they proved that the use of stimuli-responsive nanocarriers to embed MBT molecules represents a feasible approach to tackle this problem. In the present work, we aim to extend this strategy to another heterocyclic corrosion inhibitor, namely benzotriazole (BTA), which is particularly effective for the protection of copper-based alloys [12], and which is also largely exploited in the field of cultural heritage preservation [10]. Benzotriazole molecules form a strongly bonded chemisorbed two-dimensional barrier film of less than 50 angstroms, which protects copper and its alloys in aqueous media and various aggressive environments. In the literature, only a few works deal with the photodegradation stability of BTA, and it still remains a topic of debating, although BTA is the main anticorrosion component of commercial lacquers that are widely used for the protection of works of art made of copper-based alloys. However, we have verified that UV-induced degradation causes a significant lowering of the anticorrosion efficacy of the BTA molecules. Nonetheless, the encapsulation of the corrosion inhibitors into mesoporous silica nanoparticles (MSN), which can be dispersed in the coating matrix, allows to preserve them from photodegradation.

In addition, with a proper designing of the MSN, the BTA molecules can be released in the coating only in the presence of acid-related stimuli, such as a change of pH. As a result, the present study proves that polymer nanocomposite coatings containing functionalized MSN ensure a long-lasting and reliable protection against corrosion, and are thus suitable for cultural heritage preservation purposes.

2. Experimental

2.1. Materials

Metacril, a commercial acrylic resin in organic solvent (dry content 20-25 wt%) containing 1.5 wt% benzotriazole (BTA), was obtained from Antichità Belsito (Rome, Italy).

Tetraethyl orthosilicate (TEOS, reagent grade 98%), cetyltrimethylammonium bromide (CTAB, ≥ 99%), triethanolamine (TEA, ≥ 99%), benzotriazole (BTA, ReagentPlus®, 99%), copper (II) sulphate pentahydrate (ACS reagent, ≥ 98.0%), hydrochloric acid (ACS reagent, 37%), potassium hydroxide (pellets, Emplura®), acetone (≥ 99.9%), and ethanol (≥ 99.8%), were obtained from Sigma Aldrich (Milan, Italy).

Copper-based alloy disks (diameter: ~30 mm, thickness: ~5 mm) were used as metal substrate. The concentration of the main alloying elements of copper was: 4.48 wt% of Sn, 5.32 wt% of Zn and 5.24 wt% Pb, 0.10 wt% of Fe and 0.02 wt% of Ni [13]. Bi-distilled water was used for all the laboratory procedures.

2.2. Preparation of samples

Synthesis of MSN. Plain MSN nanoparticles were prepared using CTAB as a surfactant and TEA as mineralizing agent. CTAB was dissolved in a mixture of distilled water and TEA and the mixture was stirred for 1 h at 80°C. Then TEOS was quickly added and the mixture was stirred for further 2 h. The synthesis was performed with CTAB, TEA, H_2O and TEOS in the molar composition 0.06:8:80:1. The product of the reaction was easily collected through filtration, washed with water and calcined at 600 °C for 6 h.

Loading of MSN with BTA. The loading of BTA onto MSN was performed using the following procedure. BTA was dissolved in acetone at room temperature (100 mg/mL) and let to adsorb onto MSN nanoparticles previously dried under vacuum overnight. The loading procedure was repeated 3 times in order to increase the loading efficiency. MSN loaded with BTA were then treated with water at 40°C for 1 h under mechanical stirring to remove the excess of BTA and nanoparticles were centrifuged at 10.000 rpm for 10 min at 40 °C, then frozen by treatment with liquid nitrogen and

lyophilized. The obtained product was coded as MSN-BTA and contains about 21 wt% of BTA (please see below for more details).

MSN-BTA stopper formation. MSN-BTA (350 mg) were added to 70 mL of a water solution of copper sulphate (20 mM), kept under mechanical stirring for 2 min, then centrifuged at 10.000 rpm for 10 min. The solution was removed, and the nanoparticles were washed with water, separated by centrifugation, frozen in liquid nitrogen and lyophilized. The obtained product was coded as F-MSN.

Active coating preparation. The formulation for the nanocomposite coating (hereinafter referred to as F-MSN/acrylic) was prepared by adding F-MSN (5 w/w% with respect to the amount of polymer) to the commercial product Metacril previously diluted in xylene in order to get a final polymer concentration of about 1.5 w/v%. Ultrasonication was used to homogenously disperse the particles in the polymeric solution. For the sake of comparison, a coating containing the same amount of corrosion inhibitor molecules freely dispersed in the polymer matrix (hereinafter referred to as BTA/acrylic) was obtained by adding the proper amount of BTA to the diluted Metacril solution. In both the coating formulations, the total content of BTA was equal to 2.5 wt% with respect to the amount of polymer. Coatings with only corrosion inhibitor molecules adsorbed on the metal surface (i.e. without polymer) were also prepared by using aqueous solutions of BTA (~ 2 mg/L). In any case, before coating deposition the copper-based alloy substrates were cleaned with SiC papers and diamond pastes to obtain a smooth surface with a mirror-like finishing. Then, the coatings were deposited by drop-casting, followed by spreading of the solution with the tip of the pipette to cover the entire metal surface. This deposition method was selected because it resembles the brushing approach that is often adopted for the preservation of works of art. The amount of solution to deposit on the disk surface was selected in order to obtain very thin coatings (about 2 microns in thickness) so as not to alter the aesthetic properties of the underlying metal substrates, which is an essential requisite when dealing with work of art.

2.3. Characterization

Textural properties of MSN. Nitrogen adsorption analysis was performed on MSN to evaluate the textural properties of the nanocarriers. BET (Brunauer-Emmett-Teller) specific surface area (SSA) was evaluated by N_2 adsorption at 77 K through a Micromeritics ASAP 2020 analyzer (Norcross, GA, USA). Pore size distribution was evaluated using the Barrett, Joyner, and Halenda (BJH) method. The adsorption measurements were performed using high purity gases (> 99.999%). MSN were degassed at 150 °C under vacuum before analysis ($P < 10^{-5}$ mbar).

Transmission electron microscopy (TEM) analysis. Bright field TEM analysis was performed on MSN, MSN-BTA and F-MSN. For each sample, specimens were collected by mild sonication of

nanoparticles in ethanol with a Sonics Vibracell (Newtown, CT, USA) ultrasonic processor (500 W, 20 kHz) at 25% of amplitude for 3 min, then carbon coated copper grids were immersed into the dispersions and dried at room temperature. TEM analysis was performed using a FEI Tecnai G12 Spirit Twin (LaB6 source) at 120 kV acceleration voltage (FEI, Eindhoven, The Netherlands). TEM images were collected on a FEI Eagle 4 k CCD camera.

Thermogravimetric analysis (TGA). TGA was performed on MSN and F-MSN samples by means of a Perkin Elmer Pyris Diamond TG/DTA (Waltham, MA, USA) in air flow using a heating rate of 20 °C/min.

Release tests. The release of BTA from the smart nanocarriers in water at pH 7 and in HCl water solution (pH 1.5) was tested at 25 °C. F-MSN were dispersed in water (pH 7) and in HCl solutions (at pH 1.5 and 4.5) at the concentration of 0.030 mg/mL and the release of BTA in water was monitored by UV spectrophotometry. The analysis was conducted on a Jasco V570 UV spectrophotometer (Jasco, Easton, MD, USA). Calibration curves were collected at different pH values to determine the BTA concentration from the absorbance of the band between 220 and 300 nm.

Accelerated corrosion tests. UV-induced photodegradation of BTA molecules was carried out in a home-made UV irradiation apparatus emitting UV radiations (350-400 nm). Aqueous solutions of BTA (~ 2 mg/L) were exposed to UV irradiation in order evaluate the inhibitor photodegradation kinetics. UV-vis spectra of the solutions aliquots were recorder at different time intervals on an Agilent Cary 60 UV/Vis spectrophotometer (Agilent, Santa Clara, CA, USA). Disks coated with only BTA and with the polymeric coatings were also subjected to UV irradiation to study the effect of BTA photodegradation on its ability to provide anticorrosion protection and to assess the possibility of preserving BTA molecules by using mesoporous silica particles as nanocarriers. The protective ability of the coatings was assessed by accelerated corrosion tests. The disks were exposed to acid vapors of aqueous HCl solutions (at different concentrations) at 50°C. The detailed procedure can be found elsewhere [14]. Note that the adopted testing conditions have been already proved to be suitable to assess the anticorrosion protection of different kinds of organic coatings on copper-based alloys [6, 9, 13, 15].

Morphological analysis. The advancement of corrosion processes is characterized by the formation of corrosion products on the metal surface which was inspected through optical microscopy. In details, an optical microscope Olympus BX51 (Olympus, Waltham, MA, USA) was used to investigate the morphology of the BTA coated copper-based alloy disks, while a Lynx EVO stereomicroscope (Vision Engineering Ltd, Milan, Italy) was used to investigate the state of corrosion of the F-MSN/acrylic and BTA/acrylic coated disks. Moreover, the metal disks coated with F-

MSN/acrylic and BTA/acrylic were also investigated using a FEI Quanta 200 FEG scanning electron microscope (SEM) (FEI, Eindhoven, The Netherlands) in low vacuum mode at P_{H2O} = 0.60 torr. The samples were observed at 10-20 kV acceleration voltage using a secondary electron detector. Energy dispersive X-ray (EDX) point mode and mapping analysis was performed on the coating surfaces by means of the above-mentioned SEM equipped with an Inca Energy System 250 and an Inca-X-act LN2-free analytical silicon drift detector (Oxford Instruments, Abingdon-on-Thames, UK).

3. Results and discussion

Many corrosion inhibitor molecules are subjected to UV-induced photodegradation processes, which affects their protective ability. In particular, exposed to UV light, BTA may undergo to a series of photo-induced reactions. The complex degradation pathways of BTA under UV-induced photodegradation have been deeply investigated [11, 16, 17]. In agreement with literature data, the photodegradation of BTA in aqueous solution brings about significant changes of its UV-vis spectrum (Figure 1). In particular, an increase of the optical density is observed at low wavelengths, mainly as a consequence of the rise of a new absorption peak around 240-250 nm. On the other hand, the characteristic peak of unaged BTA, which is located at ~ 260 nm, seems unchanged over time. As a result, the maximum absorbance shifts towards lower wavelengths (i.e. around 254 nm) of the and there is an overall increase of the optical density in the 225-275 nm wavelength range. With respect to previously reported literature data, in our conditions the formation of a new absorption band centered at about 430 nm, assigned to the primary intermediate produced by the N–NH bond scission [18] was not observed. Nevertheless, it is worth noting that, in order to simulate real conditions, the data shown in Figure 1 were collected on aerated solutions, i.e. in presence of oxygen. Indeed, when corrosion inhibitors are used within organic coatings, the diffusion of oxygen from the surrounding environment should be taken into account, as it can provide an accelerating effect on the photolysis processes. In the adopted conditions, the presence of oxygen could reduce the stability and thus prevent the revealing of intermediate degradation products. Although it is not easy to rationalize the process, the results shown in Figure 1 confirm that the BTA undergoes to specific photo-degradation reactions during the exposure to UV light.

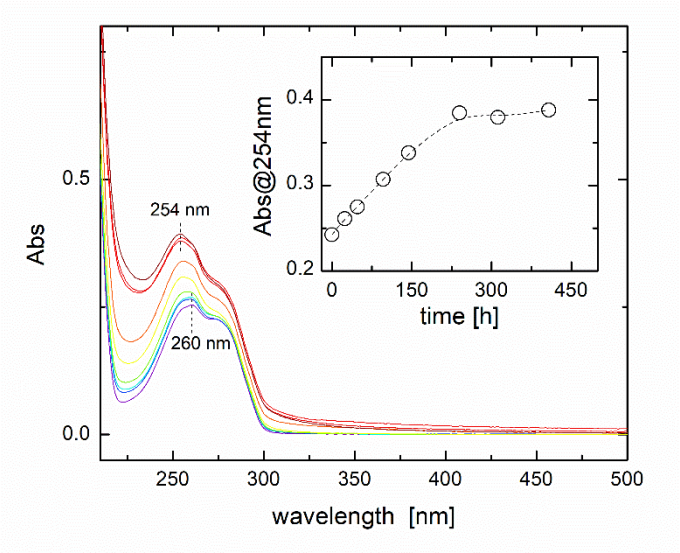

Figure 1. UV-vis spectra of BTA in air-saturated water solution after UV exposure of different duration. The time evolution of the characteristic absorbance of the new peak at 254 nm is shown in the inset.

To assess the effect of such BTA photodegradation on its anticorrosion ability, metal disks were coated with as-prepared and UV irradiated (450 h) aqueous solutions of BTA, and then subjected to accelerated corrosion tests. After only 15 mins of exposure to acid vapors (0.1 M HCl at 50°C) the uncoated disk showed severe formation of corrosion products, which can be recognized as the black spots in optical micrographs reported in Figure 2a. As shown in Figure 2b, the presence of unaged BTA molecules adsorbed at the metal surface is highly effective in preventing corrosion. Nonetheless, their corrosion inhibition ability is detrimentally affected by UV irradiation, as testified by the appearance of dark corroded areas in Figure 2c.

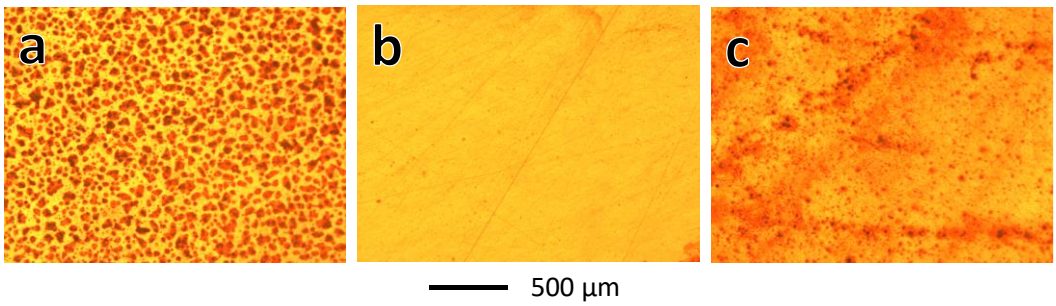

Figure 2. Optical microscope images of a) uncoated copper-based alloy disk and disks coated with b) BTA and c) UV-irradiated BTA after 15 min of accelerated corrosion treatment with 0.1M HCl at 50°C.

In the light of the results shown in Figure 2, it clearly emerges that UV-induced photodegradation of BTA must be avoided if the goal is the development of long-lasting and highly protective coatings. With this aim, MSN were synthesized and used as possible smart nanocarriers for preventing BTA molecules from exposure to UV irradiation. Furthermore, MSN were properly designed and functionalized to promote the stimuli-responsive release of the inhibitor in presence of a corrosive acid agent.

Plain MSN were obtained by a facile high-throughput synthesis, with a 98 % yield [19]. Volumetric nitrogen adsorption measurements showed that MSN have a BET SSA of 620 ± 10 m^2/g, and are characterized by a micro/mesoporous texture with a total porosity of 0.57 cm^3/g. The nitrogen isotherm of MSN, reported in Figure 3a, appears as a type IV isotherm with an unusual adsorption at very low relative pressure. At very low pressure, in fact, the steep increase of the N_2 isotherm is representative of the presence of narrow micropores, while the following sharp step between 0.2 and 0.4 p/p^0 is characteristic of 2-3 nm mesopores. The desorption branch of the isotherm coincides with the adsorption branch, showing no hysteresis, in compliance with the presence of only narrow mesopores.[20, 21].

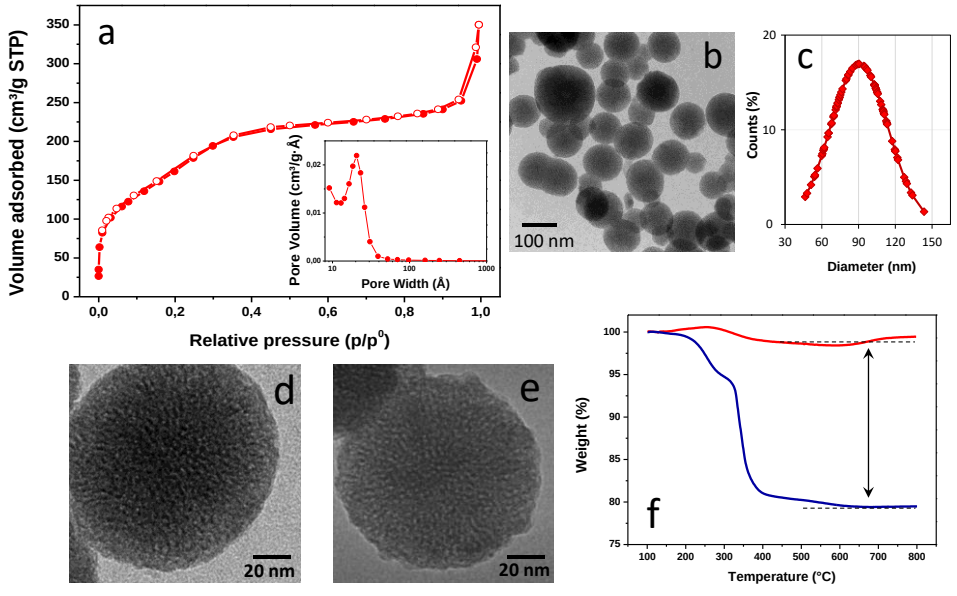

Figure 3. Nitrogen adsorption/desorption isotherms of MSN (a, BJH pore size distribution in the inset); TEM image of MSN (b); size distribution of MSN (c); higher magnification TEM images of MSN and F-MSN (d, e); TGA traces of MSN (red curve) and F-MSN (blue curve) (f).

TEM analysis revealed for MSN a very homogeneous size distribution (Figure 3b). The size distribution of the nanoparticles was determined from image analysis, revealing that the MSN diameters ranges between 49 and 143 nm with an average value of 90 ± 24 nm. The diameter distribution of MSN is reported in Figure 3c. Moreover, high magnification TEM analysis clearly revealed the worm-like mesoporous structure of the nanoparticles, well evidenced by the presence of interconnected channels (Figure 3d).

An effective procedure was then set up to load plain MSN with BTA. The loading efficiency was optimized by letting a high concentrated BTA solution in acetone adsorb onto previously dried under-vacuum MSN nanoparticles. The loading procedure was repeated 3 times. After washing to remove the excess of BTA, a "stopper" was applied to reduce the BTA release in water at neutral conditions and to promote the release of BTA from the nanoparticles only in response to an external stimulus, such acid solutions at different concentration. The formation of stoppers for BTA loaded onto the mesoporous nanocarriers was based on the reaction between loaded BTA and copper ions, which diffused into MSN to form insoluble BTA-Cu polymeric complexes [22, 23], that close the BTA-filled pores hindering the release of pristine BTA molecules. This complex exhibits a very low solubility at neutral pH with higher effectiveness in closing the pores. A TEM micrograph representative of F-MSN nanoparticles is shown in Figure 3e, indicating that the BTA-Cu complex does not significantly modify the morphology of MSN. BTA is almost homogeneously distributed within the nanoparticle with a slight accumulation on the nanoparticle surface. This external accumulation allows the formation of a diffuse BTA-Cu shell which contributes to hinder the release of pristine BTA from pores. To obtain a quantitative evaluation of BTA loading, MSN and F-MSN were analysed by means of TGA. As shown in Figure 3f, F-MSN have a residual weight at 700 °C significantly lower than MSN, due to the thermoxidative degradation of the organic component. From TGA measurements, the amount of BTA loaded onto the MSN nanoparticles was estimated equal to 21 ± 4 wt%. Based on the MSN total porosity and considering the BTA density, the theoretical maximum BTA loading would be about 43.5 wt%. Therefore, the achieved loading of BTA represents about 50% of the maximum loading capacity.

The stopping procedure based on the formation of the BTA-Cu complex was already proven to be responsive to treatments with basic solutions using halloysite nanotubes as nanocarriers, from which the release of BTA can be effectively modulated by changing the pH in the range 8-14 [23]. In the present work, the release of BTA from the copper complex was investigated and exploited in acid conditions. Indeed, as shown in Figure 4a, F-MSN release about 20 wt% of the adsorbed BTA at pH 7, and over 90 wt% at pH 1.5 for HCl. This is explained by considering the high solubility of the

BTA-Cu complex in acid conditions, clearly shown by the images of Figures 4b and c, where a BTA solution treated with copper sulphate is shown at pH 7 (Figure 4b) and at pH 1.5 (Figure 4c).

For what concerns the release kinetics, it is to be underlined that the release rate of BTA in HCl solutions is pH dependent. As shown in Figure 4a, at pH 1.5 the release is very fast, as more than 70 wt% of the BTA contained in the nanoparticles is released in the first 2 minutes of the test and the plateau is reached in about 40 min of test. Instead, at pH 4.0 the release is much slower, about 70 wt% of the BTA contained in the nanoparticles is released in 40 min, and the plateau is reached only after more than 180 min of test. The obtained results confirm that the nanoparticles exhibit a BTA release which depends on the concentration of the external acid, following the mechanism proposed in Figure 4d: at very low pH values the external layer composed by the BTA-Cu complex is quickly dissolved and the release of BTA from the nanoparticle pores proceeds very fast. At higher pH values, the BTA-Cu complex is more resistant to the acidic attack and the release of BTA from the silica pores is slowed down. This feature is very important because it allows to regulate the anticorrosion release accordingly to the degradation process of the copper-based alloy, which is expected to be a first order reaction with respect to the concentration of chloride.

To evaluate the corrosion inhibitor efficiency of the F-MSN, the nanoparticles were dispersed into a commercial acrylate protective formulation, a class of material widely used in conservation of cultural heritage although their limited resistance to UV exposure [24,25]. and this formulation was used to realize protective coatings (coded F-MSN/acrylic) on copper-based alloy disks. For comparison, coatings containing only free BTA (coded BTA/acrylic) were also realized. Metal disks coated with F-MSN/acrylic and BTA/acrylic were aged by prolonged UV irradiation and then tested by accelerated corrosion tests by exposure to the vapours of acid solutions with different pH and for different times. Results are summarized in Figure 5. Before and after UV irradiation, both coatings showed high transparency (see Figures 5a, b and f, g), even if F-MSN nanoparticles are characterized by a pale blue colour. By exposure to the vapours of a 1 M HCl solution at 50 °C, both coatings show quite good protection of the metallic surface up to 6 hours. At this time, the first differences start to appear. The disk coated with BTA/acrylic shows the formation of small corrosion points (Figure 5c), while the disk coated with F-MSN/Met shows only a quite opacification of the disk (Figure 5h). A further 1 hour-exposure to the vapours of a 10 M HCl solution at 50 °C induces a significant enlargement of the corrosion areas on the disk coated with BTA/acrylic (Figure 5d), while no significant differences are evidenced for the F-MSN/acrylic coated disk (Figure 5i). 1 further hour of exposure to the 10 M HCl solution induces the complete covering of the BTA/acrylic coated disk with rust (Figure 5e), while the F-MSN/acrylic coating still protects the metal surface, which shows almost completely uncontaminated areas in the centre of the disk (Figure 5j).

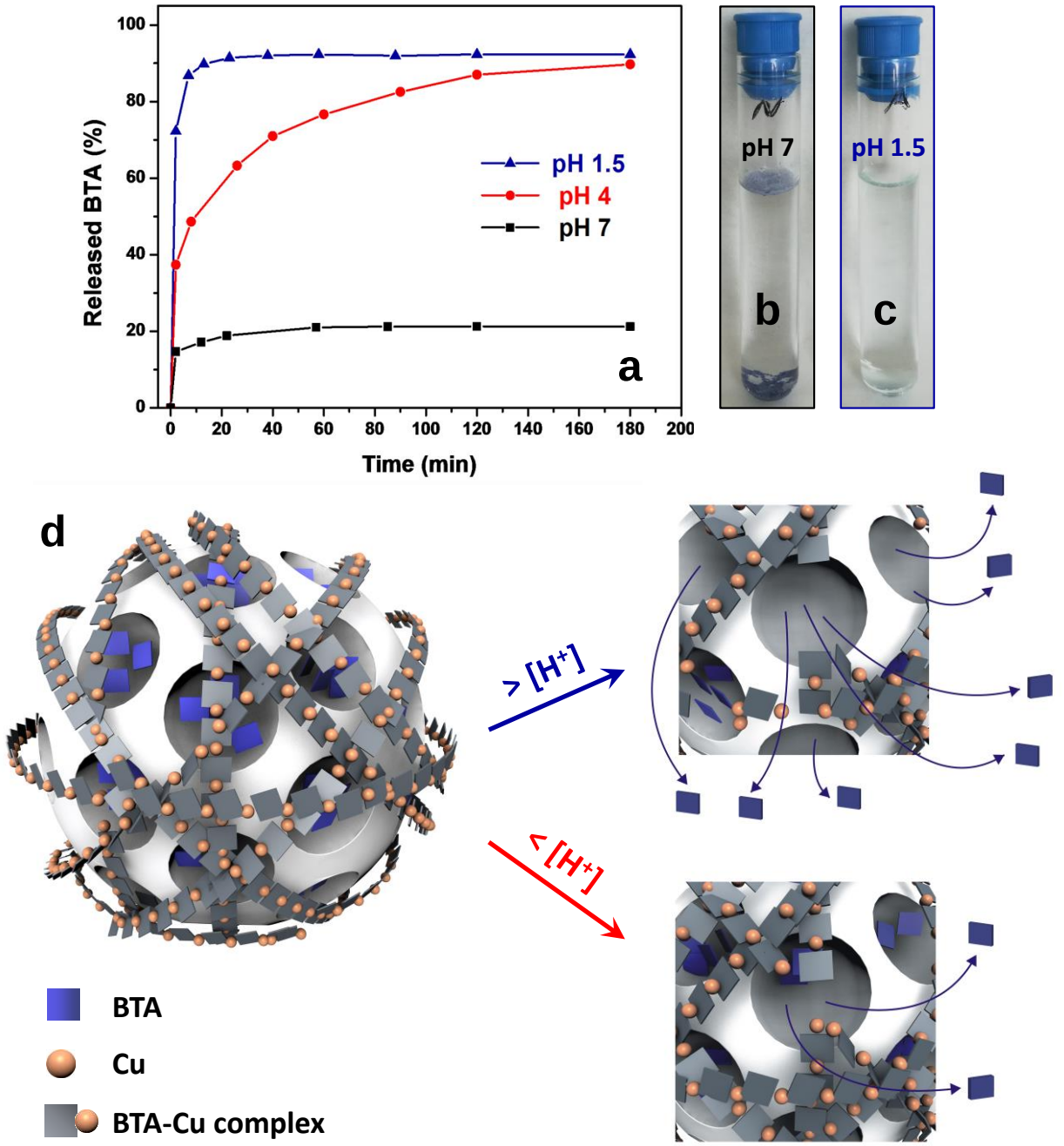

Figure 4. Release kinetics of BTA from F-MSN at different pH (a). Images of a BTA water solution treated with copper sulphate before (b) and after (c) addition of HCl. Scheme of the BTA release in acid solution at lower and higher pH values (d).

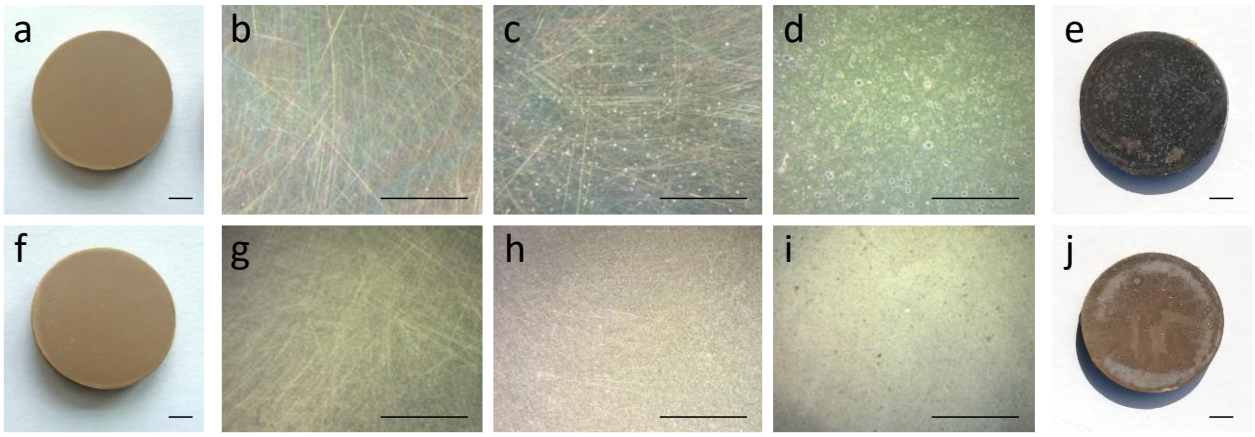

Figure 5. Pictures and optical microscope images of metal disks coated with BTA/acrylic (top raw) and F-MSN/acrylic (bottom raw). Coated disks aged by UV (a, b, f, g); coated disks after 6 h exposure to vapours of a 1 M HCl solution (c, h); coated disks after further 1 h exposure to vapours of a 10 M HCl solution (d, i); coated disks after further 1 h exposure to vapours of a 10 M HCl solution (e, j). Scale bar in all images is 5 mm.

To clarify the mechanism of formation of degraded area and thus to collect information on the mechanism of protection of the smart F-MSN nanoparticles, SEM analysis coupled to EDX was performed on the copper-based alloy disks coated with BTA/acrylic and F-MSN/acrylic at low corrosion degree, i.e. after 6 hours of exposure to the vapours of the 1M HCl solution. SEM images of the metal disk coated with BTA/acrylic, aged by UV irradiation and then exposed for 6 hours to vapours of the 1 M HCl solution are reported in Figure 6a-c. As shown, the investigated area is constituted by the polymer coating with the presence of quasi-circular large spots with a diameter of about 100 μm (Figure 6b) and small aggregates of lateral size of about 2-5 μm (Figure 6c). SEM observations at higher magnification revealed that the large spots have morphological features typical of inorganic salts and they are located on the top of the sample (inset of Figure 6b). In these regions, there is no evidence of the original polymer coating, still present in the regions outside the spots. EDX map performed on these corrosion areas (Figure 6d), confirmed the presence of the organic coatings outside the spots, where carbon was clearly revealed, and the composition of the inorganic material originated by the corrosion, that resulted a copper chloride salt. To be noted is that by EDX, copper is also found in the regions outside the spot because the low thickness of the acrylic coating is not able to mask the high presence of this element on the metal substrate. On the other hands, small

aggregates (Figure 6c) have morphological features similar to the inorganic salts found in the large spot regions, but they are clearly still covered by a polymer coating.

For what concerns the metal disk coated with F-MSN/acrylic, the presence of spots is more diffused on the disk surface, but these spots are smaller (diameter 10-40 μm, see Figure 6f) than those found on the sample coated with BTA/acrylic. Moreover in these regions a much lower amount of salt was observed and the coating, although partially wrapped, was still present (Figure 6g). Indeed, EDX map revealed the presence of carbon also inside the spots (Figure 6h). Moreover, at the investigated magnifications, silicon was almost homogeneously distributed, confirming the absence of very large silica nanoparticle agglomerates.

All these findings suggest that the mechanism of corrosion by exposure to HCl vapours of the metal substrate coated and aged by UV irradiation proceeds through the diffusion of HCl though the coating. Once HCl reaches the metal surfaces it chemically reacts with copper inducing the formation of the copper chloride, whose formation progressively damages the integrity of the polymer coating. As a consequence of the damages generated into the coating, further HCl vapours can directly reach the substrate and the corrosion mechanism becomes very fast, with the quick formation of large aggregates of copper chloride that progressively cover the whole area exposed to the acid vapours.

In presence of the smart nanocarriers containing stopped BTA, the HCl molecules probably reach the surface of the metal moving through the interfaces between nanoparticles and the acrylic coating. This brings about many small localized corrosion spots. Nonetheless, the nanocarrier protects the loaded BTA from the UV degradation and thus, once HCl starts to diffuse through the coating, it induces the release of BTA, which reacts with copper forming the well described BTA-Cu coordination compounds. These compounds act as effective inhibitor against corrosion [22], significantly slowing down the kinetic of formation of copper chloride salts onto the metal surface. The results confirm that the mesoporous silica is effective in protecting the BTA from the photodegradation and the resulting acrylic-based active coatings are thus very effective in the long-lasting stability of the copper-based alloy substrates towards acid vapors.

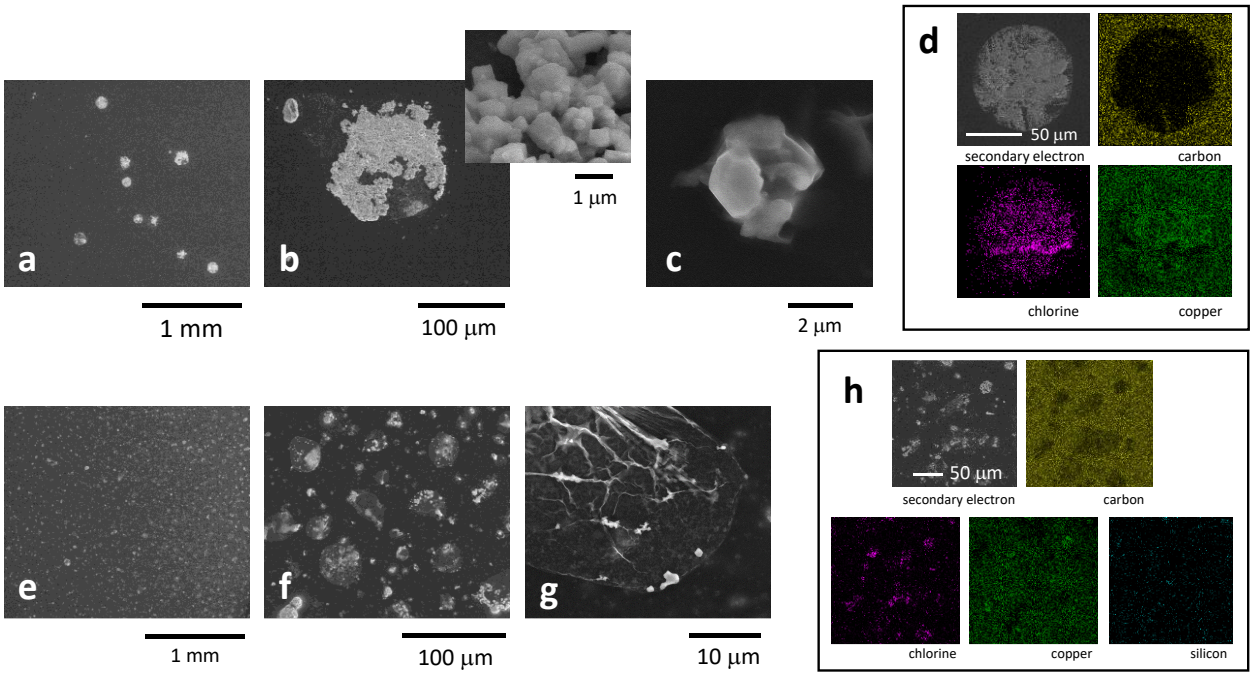

Figure 6. SEM images (a, b, c) and EDX maps (d) of a copper-based alloy disk coated with BTA/acrylic, aged by UV irradiation and then exposed for 6 hours to vapours of 1M HCl solution at 50 °C. SEM images (e, f, g) and EDX map (h) of a copper-based alloy disk coated with F-MSN/acrylic undergone to the same UV ageing, followed by the simulated corrosion treatment for 6 hours.

4. Conclusions

The protective efficacy of polymer nanocomposite coatings against corrosion phenomena in copper-based alloy substrates was investigated for applications in cultural heritage conservation. The developed coatings are based on mesoporous silica nanoparticles loaded with benzotriazole molecules as corrosion inhibitor agent. Such nanocarriers have been properly designed and functionalized in order to exhibits a controlled release of the inhibitor molecules in acidic environments. In addition, the benzotriazole molecules loaded into the nanocarriers are protected against photodegradation, and thus keep intact their anticorrosion ability. As a result, the polymer nanocomposite coatings possess reliable and long-lasting protective ability, as testified by accelerated corrosion tests carried out on coated copper-based alloy disks by exposure to vapors of hydrochloric acid water solutions.

Acknowledgments

The work was supported by the European H2020 funded Project InnovaConcrete (G.A. n. 760858). The authors acknowledge A. Aldi, F. Docimo and C. Del Barone for the technical assistance in the experiments.

References

[1] S. B. Lyon, R. Bingham, D. J. Mills, Advances in corrosion protection by organic coatings: What we know and what we would like to know, Prog. Org. Coat. 102, (2017) 2-7.

[2] D. G. Shchukin, Container-based multifunctional self-healing polymer coatings, Polym. Chem. 4, (2013) 4871-4877.

[3] J. Tedim, S. K. Poznyak, A. Kuznetsova, D. Raps, T. Hack, M. L. Zheludkevich, M. G. S. Ferreira, Enhancement of active corrosion protection via combination of inhibitor-loaded nanocontainers, ACS Appl. Mater. Interf. 2, (2010) 1528-1535.

[4] E. Abdullayev, V. Abbasov, A. Tursunbayeva, V. Portnov, H. Ibrahimov, G. Mukhtarova, Y. Lvov, Self-healing coatings based on halloysite clay polymer composites for protection of copper alloys, ACS Appl. Mater. Interf. 5, (2013) 4464-4471.

[5] J. Fu, T. Chen, M. Wang, N. Yang, S. Li, Y. Wang, X. Liu, Acid and alkaline dual stimuli-responsive mechanized hollow mesoporous silica nanoparticles as smart nanocontainers for intelligent anticorrosion coatings, ACS Nano 7, (2013) 11397-11408.

[6] M. Salzano de Luna, G. G. Buonocore, C. Giuliani, E. Messina, G. Di Carlo, M. Lavorgna, L. Ambrosio, G. M. Ingo, Long-Lasting Efficacy of Coatings for Bronze Artwork Conservation: The Key Role of Layered Double Hydroxide Nanocarriers in Protecting Corrosion Inhibitors from Photodegradation, Angew. Chem. Int. Ed. 57, (2018) 7380-7384.

[7] C. J. McNamara, M. Breuker, M. Helms, T. D. Perry, R. Mitchell, Biodeterioration of Incralac used for the protection of bronze monuments, J. Cult. Herit. 5, (2004), 361-364.;

[8] E. Kiele, J. Lukseniene, A. Griguceviciene, A. Selskis, J. Senvaitiene, R. Ramanauskas, R. Raudonis, A. Kareiva, Methyl–modified hybrid organic-inorganic coatings for the conservation of copper, J. Cult. Herit. 15, (2014) 242-249.

[9] C. Giuliani, M. Pascucci, C. Riccucci, E. Messina, M. Salzano de Luna, M. Lavorgna, G. M. Ingo, G. Di Carlo, Chitosan-based coatings for corrosion protection of copper-based alloys: a promising more sustainable approach for cultural heritage applications, Prog. Org. Coat. 122, (2018) 138-146.

[10] P. Dillmann, D. Watkinson, E. Angelini, A. Adriaens (Eds.), Corrosion and conservation of cultural heritage metallic artefacts, Elsevier (2013).

[11] M. Serdechnova, V. L. Ivanov, M. R. M. Domingues, D. V. Evtuguin, M. G. Ferreira, M. L. Zheludkevich, Photodegradation of 2-mercaptobenzothiazole and 1, 2, 3-benzotriazole corrosion inhibitors in aqueous solutions and organic solvents, Phys. Chem. Chem. Phys. 16, (2014) 25152-25160.

[12] M. Finšgar, I. Milošev, Inhibition of copper corrosion by 1, 2, 3-benzotriazole: a review, Corr. Sci. 52, (2010) 2737-2749.

[13] M. Mihelčič, M. Gaberšček, G. Di Carlo, C. Giuliani, M. Salzano de Luna, M. Lavorgna, A. K. Surca, Influence of silsesquioxane addition on polyurethane-based protective coatings for bronze surfaces, Appl. Surf. Sci. 467, (2019) 912-925.

[14] F. Faraldi, B. Cortese, D. Caschera, G. Di Carlo, C. Riccucci, T. De Caro, G. M. Ingo, Smart conservation methodology for the preservation of copper-based objects against the hazardous corrosion, Thin Solid Films, 622, (2017) 130-135.

[15] M. Mihelčič, M. Gaberšček, M. Salzano de Luna, M. Lavorgna, C. Giuliani, G. Di Carlo, A. K. Surca, Effect of silsesquioxane addition on the protective performance of fluoropolymer coatings for bronze surfaces, Mater. Design 178, (2019) 107860.

[16] H. Wang, C. Burda, G. Persy, J. Wirz, Photochemistry of 1H-Benzotriazole in Aqueous Solution: A Photolatent Base, J. Am. Chem. Soc. 122, (2000) 5849-5855.

[17] M. J. Paterson, M. A. Robb, L. Blancafort, A. D. DeBellis, Theoretical Study of Benzotriazole UV Photostability: Ultrafast Deactivation through Coupled Proton and Electron Transfer Triggered by a Charge-Transfer State. J. Am. Chem. Soc. 126, (2004) 2912-2922.

[18] Y. Ding, C. Yang, L. Zhu, J. Zhan, Photoelectrochemical activity of liquid phase deposited TiO2 film for degradation of benzotriazole, J. Hazard. Mater. 175, (2010) 96–103.

[19] K. Zhang, L.-L. Xu, J.-G. Jiang, N. Calin, K.-F. Lam, S.-J. Zhang, H.-H. Wu, G.-D. Wu, B. Albela, L. Bonneviot, P. Wu, Facile Large-Scale Synthesis of Monodisperse Mesoporous Silica Nanospheres with Tunable Pore Structure, J. Am. Chem. Soc. 135, (2013) 2427-2430.

[20] M. Thommes, K. Kaneko, A. V. Neimark, J. P. Olivier, F. Rodriguez-Reinoso, J. Rouquerol, K. S. Sing, Physisorption of Gases, with Special Reference to the Evaluation of Surface Area and Pore Size Distribution (IUPAC Technical Report), Pure Appl. Chem. 87, (2015) 1051-1069.

[21] M. Grün, K. K. Unger, A. Matsumoto, K. Tsutsumi, Novel pathways for the preparation of mesoporous MCM-41 materials: control of porosity and morphology, Micropor. Mesopor. Mater. 27, (1999) 207-216.

[22] N. K. Allam, A. A. Nazeer, E. A. Ashour, A review of the effects of benzotriazole on the corrosion of copper and copper alloys in clean and polluted environments, J. Appl. Electrochem. 39, (2009) 961-969.

[23] E. Abdullayev, R. Price, D. Shchukin, Y. Lvov, Halloysite tubes as nanocontainers for anticorrosion coating with benzotriazole, ACS Appl. Mater. Interf. 1, (2009) 1437-1443.

[24] M. Cocca, L. D'Arienzo, L. D'Orazio, G. Gentile, C. Mancarella, E. Martuscelli, C. Polcaro, Water dispersed polymers for textile conservation: a molecular, thermal, structural, mechanical and optical characterization, J. Cult. Heritage 7 (2006) 236-243

[25] M. Cocca, L. D'Arienzo, L. D'Orazio, G. Gentile, E. Martuscelli, Polyacrylates for conservation: chemico-physical properties and durability of different commercial products, Polym. Test. 23 (2004) 333-342